Supplementary Information

Metal ion and Electrolyte free Twin Electrode Photocapacitor Possessing Ultrafast Charging Capability

Karan Surana[1], Sanjay N. Bariya[1], Darshna B. Kanani[1], and Saurabh S. Soni[1,2,*]

[1]Department of Chemistry, Sardar Patel University, Vallabh Vidyanagar 388120, Gujarat, India

[2]Department of Applied and Interdisciplinary Sciences (IICISST), Sardar Patel University, Vallabh Vidyanagar 388120, Gujarat, India

*Correspondence: soni_b21@yahoo.co.in, saurabh_soni@spuvvn.edu

Materials and Methods

The synthesis of reduced graphene oxide (rGO) was performed by microwave irradiation method. Few mg of graphite flakes were subjected to microwave irradiation at 600 W for 60 s followed by ultrasonication in a mixture of methanol and double (DD) water for several hours. The obtained graphene oxide was dried and treated with hydrazine monohydrate (Alfa Aesar) and finally washed and filtered until pH neutral to obtain rGO. To prepare the rGO solution, 0.1 mg of rGO powder was dissolved in 2 mL of N-methyl-2-pyrrolidone (NMP) by probe sonication for several minutes until a clear dispersion was obtained.

The synthesis of CdSe QD was performed by wet chemical method wherein the Se precursor was prepared by refluxing sodium sulfite (Na_2SO_3) and selenium (Se) in a round bottom flask for two hours. The prepared Na_2SeSO_3 solution was filtered and poured into a beaker containing $Cd(NO_3)_2$ and 2-mercaptoethanol heated at ~ 50 °C. The prepared CdSe solution was filtered and diluted in access ethanol for extracting the QD. For application in device, the extracted CdSe QD powder was mixed in a polymer host matrix as indicated below.

For the active layer, 0.35 g of Pluronic F-127 was taken with 10% of CdSe QD and rest acetonitrile (ACN) to make the final weight 1 g. The mixture was alternated between fridge and room ambient condition every few hours for proper mixing.

All the device measurements were performed using CHI 660E electrochemical workstation. For generating 1 sun illumination (1000 W.m^{-2}) PET solar simulator #SS80AAA was utilized. UV-Vis absorption study was performed using Shimadzu UV-1800 spectrophotometer. The TEM images were obtained using JEOL JEM 2100F field emission gun TEM at an operating voltage of 200 kV by placing the sample on a lacey grid. In case of LED illumination, Syska 15W White LED lamp was used. Field emission gun scanning electron microscopy (FEG-SEM) was performed with Nova Nano FEG-SEM 450. For FEG-SEM cross-sectional images, the sample was prepared on glass

slide by spin-coating successive layers of TiO_2, rGO, and TiO_2. The thickness of the coatings was increased by enhancing the concentration of rGO and TiO_2 solutions (twice) in order to attain proper imaging under FEG-SEM. The inverted optical microscopy images were captured using an Olympus microscope. All the measurements were performed in a closed environment at 25 °C to avoid any external influence.

The following equation was used to calculate the specific capacitance of prepared devices:

$$C_s = \frac{I}{m\frac{\Delta V}{\Delta t}}$$

where 'I' is the current applied to discharge the device (A), 'm' is the mass of the active material (g), ΔV is the potential window (V), and Δt is the discharge time (s). The obtained value would be in F/g.

The solar to output energy conversion and storage efficiency (η_c) can be calculated as per the below formular:

$$\eta_c = (E_{output} / E_{light}) \times 100\%$$

Where E_{output} refers to the discharge energy of the device in $mAVh/cm^2$ while E_{light} refers to input energy from the illumination in mWh/cm^2.

The bandgap or energy gap of the prepared CdSe QD was determined using Tauc's plot from the data obtained as per the UV-Vis absorption analysis. The corresponding Tauc's equation is

$$(\alpha h\nu) = B (h\nu - Eg)^r$$

Where 'B' is a constant, 'α' is the absorption coefficient, '$h\nu$' is the photon energy, 'Eg' is the optical band gap and 'r' is an index dependent on the nature of electronic transition responsible for optical absorption. The value of 'r' is ½ for direct allowed transitions and 2 for indirect allowed transitions [A]. Since CdSe is known to have a direct bandgap, the data plot was obtained between $(\alpha h\nu)^2$ vs $h\nu$ as shown in Figure S1.
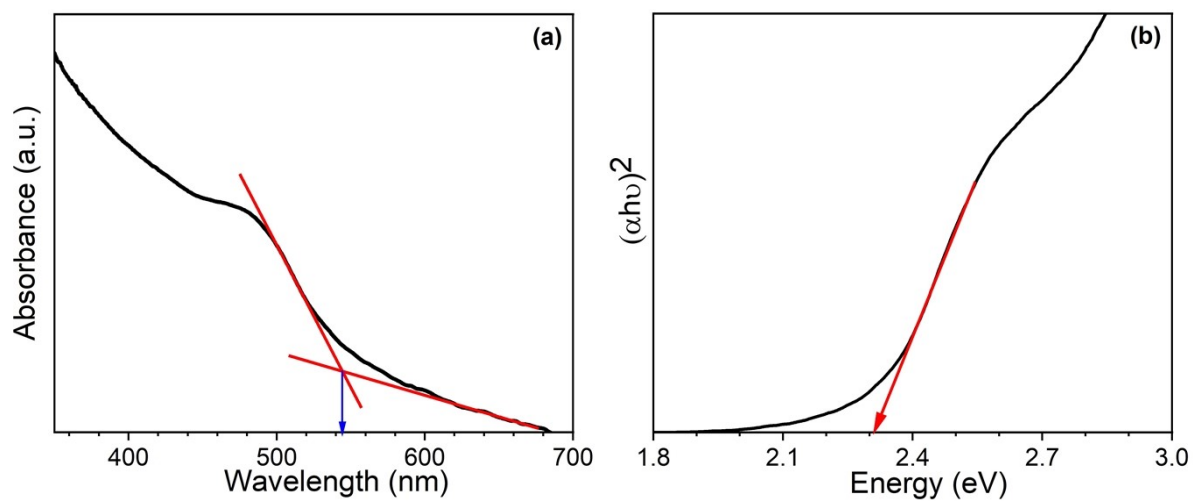
**Figure S1.** (a) Absorption onset and (b) Tauc's plot of the prepared CdSe QD
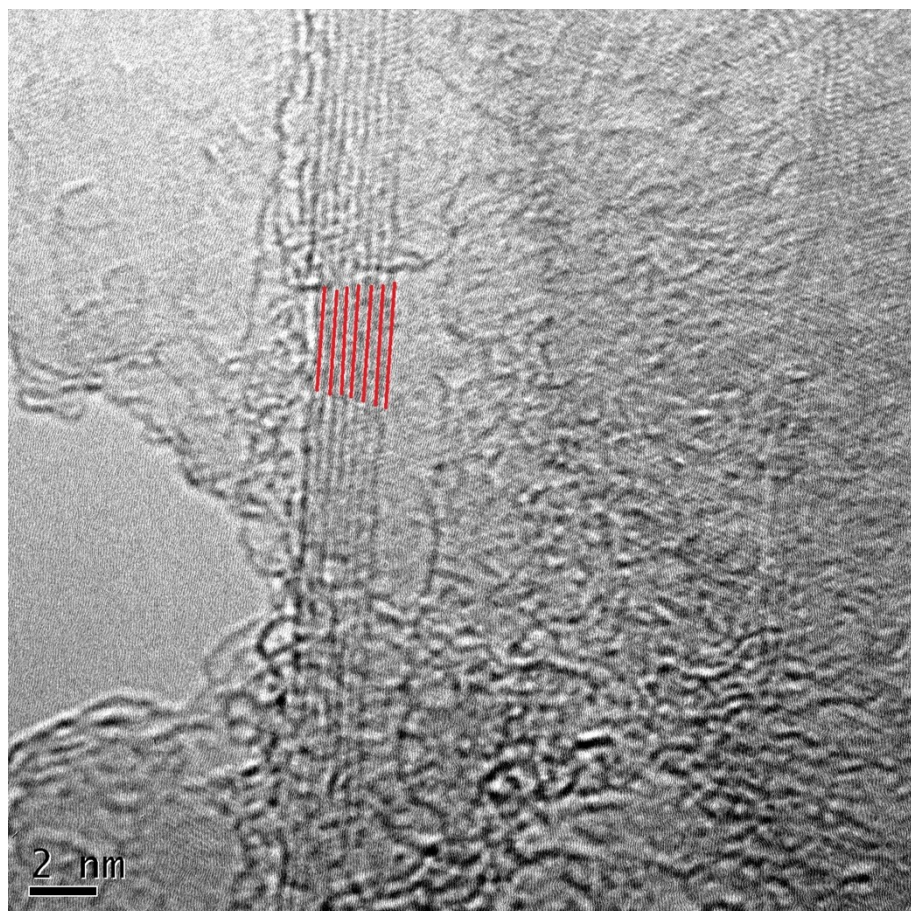
**Figure S2.** HR-TEM image of rGO depicting the sheet stacking

The prepared MLS of rGO-TiO$_2$ layers on a glass substrate was observed under an inverted optical microscope as shown in Fig. S3a and S3b. The rGO was also coated on the FTO glass without the TiO$_2$ layer for better clarity of the coated and uncoated surface. The black particles are of rGO while the rest is mesoporous TiO$_2$ as indicated in Fig. S3a. This constituted one pair of rGO-TiO$_2$ layer. Similarly, the coating of a second pair of rGO-TiO$_2$ layer is also clearly visible in Fig. S3b.
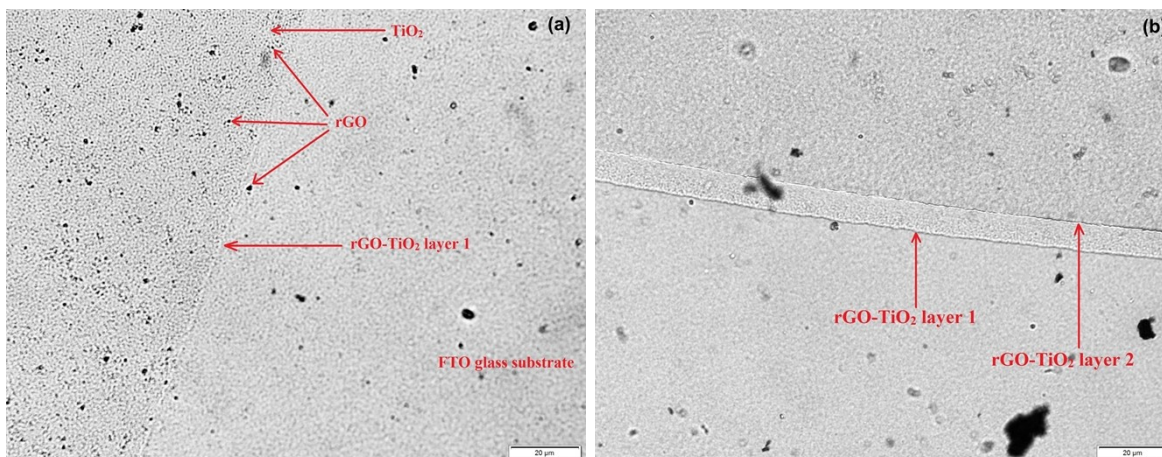

Figure S3. Optical microscopy images of (a) one pair of rGO-TiO$_2$ layer (magnification 50x) and (b) two pairs of rGO-TiO$_2$ layers (magnification 100x). Scale bar - 20 μm.
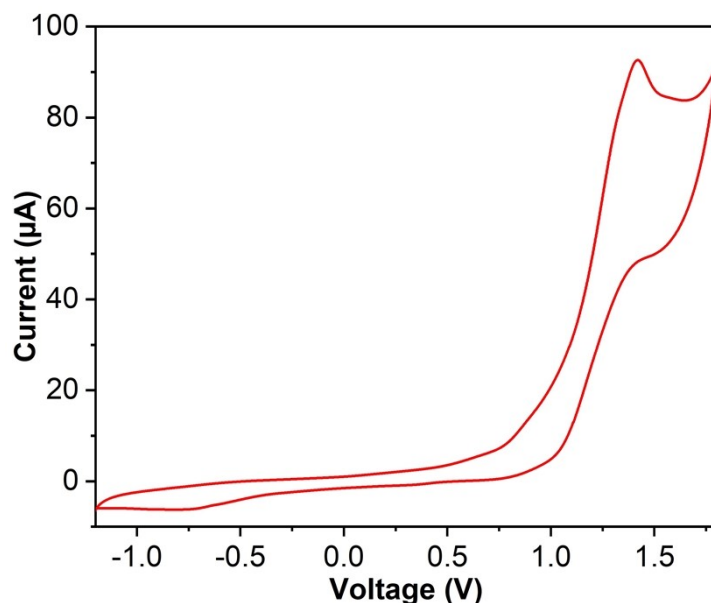
Figure S4. Two electrode CV of CdSe QD in solution phase under 1 sun illumination
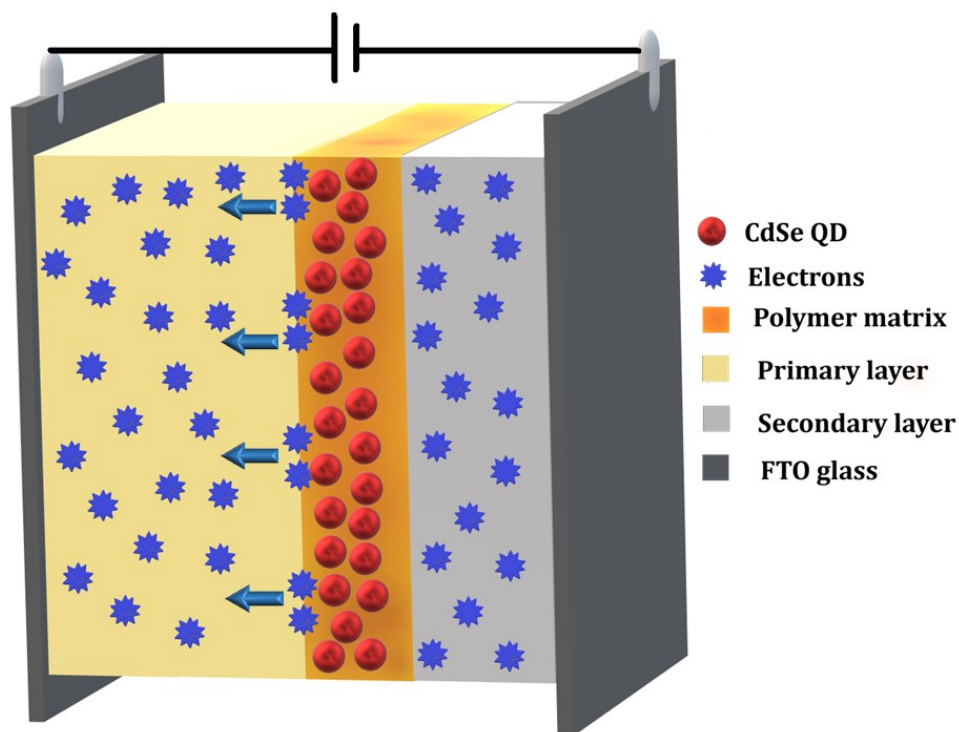
Figure S5. A schematic representation of the phenomenon relating to slight increase in potential upon turning OFF the lamp observed in Fig. 3c.
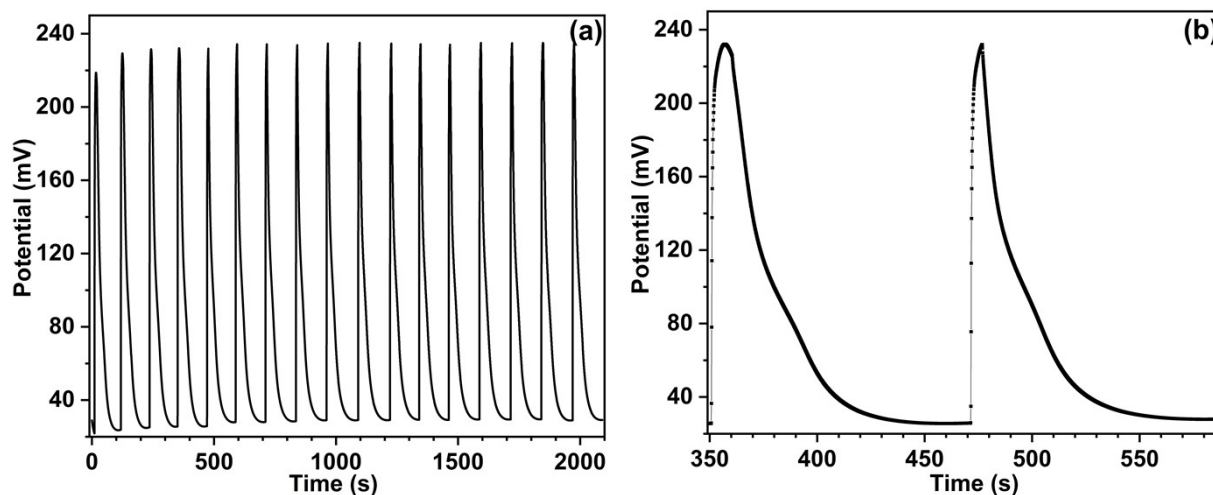
Figure S6. (a) OCVD of D-II with photo-charging time of 10 s and discharged in RA condition until the device's potential just started rising. (b) OCVD with a light irradiation time of 10 s and 5 s, respectively with discharging under RA condition. Blue star indicates light ON and maroon star indicates light OFF.
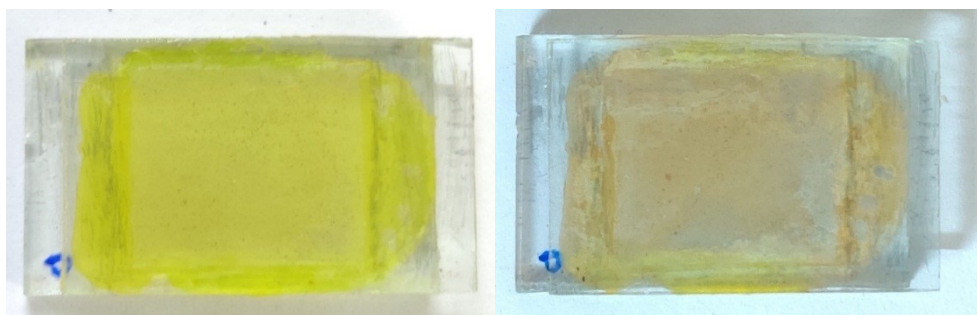
Figure S7. D-II (left) when prepared and (right) after 200 cycles of continuous photo-charging and discharging. The possible reason is the slow evaporation of the solvent which leaves unoccupied sites in the active layer. Also, the continuous oxidation and reduction of QD leads to agglomeration, thus increasing the particle size and color leading to degradation.

Table T1. Comparative study of the relevant literature to the present work

| Device Configuration	Specific Capacitance	Photo-Charging time (s)	Peak Voltage (V)	η_c (%)	Cycling stability	Ref
FTO/ZnO/Ag$_2$S/ZnS/PEDOT/ PVP-[HEMIm][BF$_4$]/PEDOT /FTO	0.667 mF/cm^2	40	0.33	8.25×10^{-4}	50	B
FTO/TiO$_2$/N719/TEABF$_4$/ MnO$_2$/CNT	13.1 mF/cm^2	2400	0.955	-	-	C
FTO/TiO$_2$/N719/I$_2$/Pt/PEDOT/ LiClO$_4$/PEDOT/Pt/FTO	0.52 F/cm^2	80	0.69	-	-	D
FTO/TiO$_2$/MAPbI$_3$/PMMA/PV A-H$_2$SO$_4$PANI/CNT	103.4 mF/g	80	0.7	0.76	-	E
FTO/TiO$_2$/CsPbBr$_3$/C/Si gel/C	33.8 mF/cm^2	3	1.2	5.1	1000	F
ITO/P3HT/ Na$_2$SO$_4$-PVA gel /ITO	2.44 mF/cm^2	50	0.28	1.7×10^{-3}	-	G
FTO/rGO-TiO$_2$/CdSe-F127/ rGO-TiO$_2$/FTO	307.4 mF/g	3 - 5	0.35	4.35×10^{-3}	200	This work

The UV-Vis absorption of multiple pairs of rGO-TiO$_2$ layers was performed and the corresponding absorption trend is shown in Figure S8. The two pairs of rGO-TiO$_2$ layers result in a smooth absorption in the visible region with an exponential rise in the UV region. The employed rGO does not show any absorption in the visible region [I]; however, it is a perfect candidate for refracting the light owing to its significant difference in RI with TiO$_2$. Focusing on the absorption of two to ten pairs of rGO-TiO$_2$ layers in the visible region (400 – 700 nm), a clear increase in the absorbance is observed up to the eighth pair followed by a decrease in the tenth pair. Since, only TiO$_2$ absorbs in the visible region while the rGO-TiO$_2$ layering causes greater number of photons to bend towards the photo-active material, an overall enhancement in the absorption can be observed. The rise in absorbance occurs up to a certain thickness (in this case eight pairs) beyond which the reduction in transparency results in loss of absorption in the visible region. This subtly justifies our hypothesis and observations for the prepared photocapacitor devices.
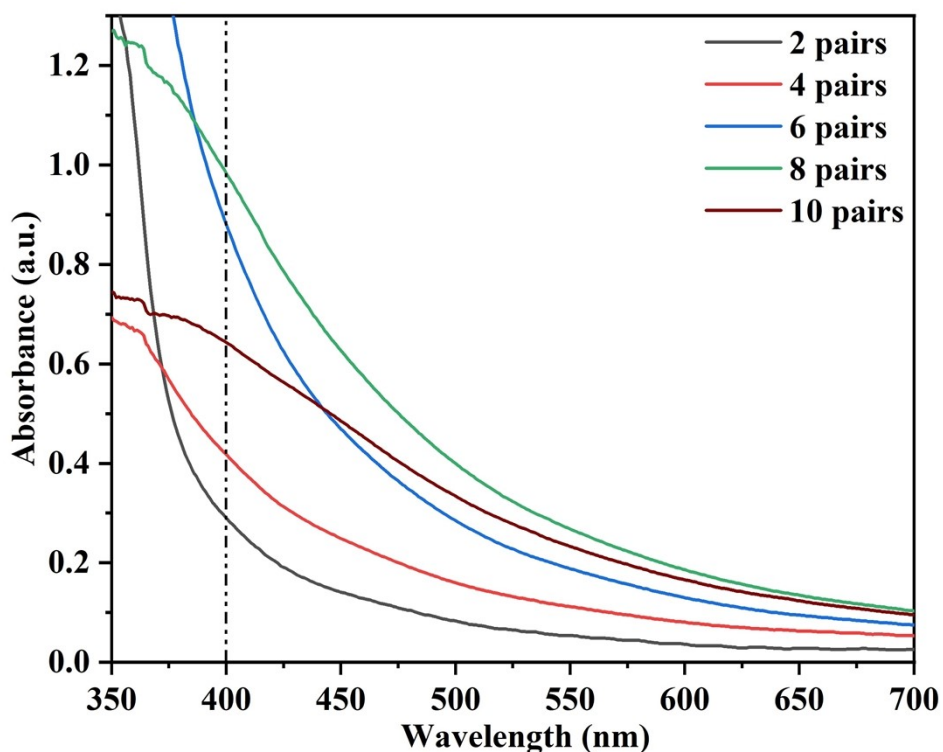

Figure S8. UV-Vis absorption of different pairs of rGO-TiO$_2$ layers coated on FTO glass. Single FTO was used for coating the layers and the UV-Vis absorption measurement was performed after each rGO-TiO$_2$ layer coating. The coating of TiO$_2$ was performed through doctor-blade technique to enable significant difference in absorption characteristics of different layers. Hence, the thickness of the rGO-TiO$_2$ layers in this measurement is greater from the ones prepared for the devices.

A comparison of the developed photo-capacitor with that of a DSSC [H] is shown in Figure S9 for better understanding of the device characteristics. A prominent contrast in the I-V pattern of the two devices can be observed. A typical photovoltaic characteristic was obtained from DSSC

wherein the generated V_{OC} is the true potential of the device while in case of D-I the generated V_{OC} is close to 1 V which is far from its true potential (~ 0.25 V, Fig. 3). Upon close observation, the obtained I-V characteristics of the device D-I is similar to its CV nature (Figure 2a) in the said range. It should be noted that the I-V measurements were also performed at the same scan rate as CV measurement (0.1 V/s). Furthermore, it is important to note that in the OCVD analysis of DSSC after light irradiation a fast decay in potential occurs, reaching close to zero potential in a time span of few seconds [H], which is not the case in the developed photocapacitor devices.
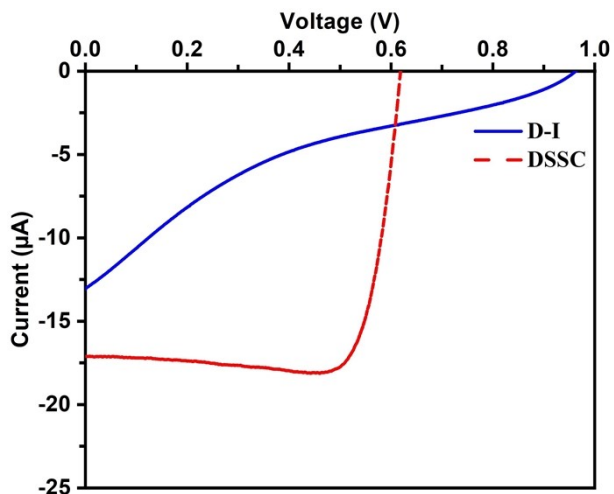
Figure S9. The I-V analysis of a conventional DSSC and D-I.
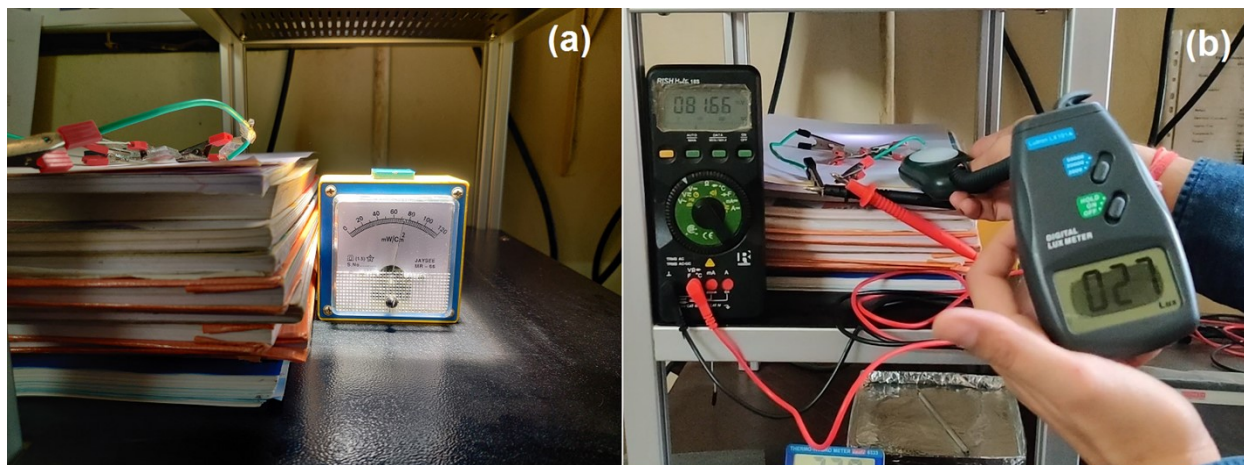
Figure S10. The devices assessed after sixty days of fabrication. (a) Xenon lamp intensity and (b) the RA light lux along with the generated potential by the devices connected in series. The responses are shown in video SV1, SV2, and SV3.

Movie SV1. The device responsiveness to room ambient light (as low as ~ 30 lx) is shown by periodically covering the device to eliminate the absorption of stray light.

Movie SV2. The charging of the device within couple of seconds upon illumination with Xenon lamp at ~ 0.8 sun condition.

Movie SV3. Time lapse video of the device charging under room ambient light (~ 30 lx).

References:

A. Surana, K., Salisu, I.T., Mehra, R.M. and Bhattacharya, B., 2018. A simple synthesis route of low temperature CdSe-CdS core-shell quantum dots and its application in solar cell. *Optical Materials*, *82*, 135-140.

B. Solís-Cortés, D., Navarrete-Astorga, E., Schrebler, R., Peinado-Pérez, J.J., Martín, F., Ramos-Barrado, J.R. and Dalchiele, E.A., 2020. A solid-state integrated photo-supercapacitor based on ZnO nanorod arrays decorated with Ag_2S quantum dots as the photoanode and a PEDOT charge storage counter-electrode. *RSC Advances*, *10*(10), 5712-5721.

C. Yilmaz, M., Hsu, S.H., Raina, S., Howell, M. and Kang, W.P., 2018. Integrated photocapacitors based on dye-sensitized TiO_2/FTO as photoanode and MnO_2 coated micro-array CNTs as supercapacitor counter electrode with $TEABF_4$ electrolyte. *Journal of Renewable and Sustainable Energy*, *10*(6).

D. Chen, H.W., Hsu, C.Y., Chen, J.G., Lee, K.M., Wang, C.C., Huang, K.C. and Ho, K.C., 2010. Plastic dye-sensitized photo-supercapacitor using electrophoretic deposition and compression methods. *Journal of Power Sources*, *195*(18), 6225-6231.

E. Liu, R., Liu, C. and Fan, S., 2017. A photocapacitor based on organometal halide perovskite and PANI/CNT composites integrated using a CNT bridge. *Journal of Materials Chemistry A*, *5*(44), 23078-23084.

F. Liang, J., Zhu, G., Wang, C., Zhao, P., Wang, Y., Hu, Y., Ma, L., Tie, Z., Liu, J. and Jin, Z., 2018. An all-inorganic perovskite solar capacitor for efficient and stable spontaneous photocharging. *Nano Energy*, *52*, 239-245.

G. Dong, W. J., Cho, W. S., & Lee, J. L. (2021). Indium tin oxide branched nanowire and poly (3-hexylthiophene) hybrid structure for a photorechargeable supercapacitor. *ACS Applied Materials & Interfaces*, 13(19), 22676-22683.

H. B. Mistry, H. K. Machhi, R. S. Vithalani, D. S. Patel, C. K. Modi, M. Prajapati, K. R. Surati, S. S. Soni, P. K. Jha, S. R. Kane, Harnessing the N-dopant ratio in carbon quantum dots for enhancing the power conversion efficiency of solar cells, *Sustainable Energy Fuels*, 3 (2019) 3182-3190.

I. K. Surana, S. H. Panjabi, D. Varade, M. P. Deshpande, U. P. Deshpande, & S. S. Soni, Low intensity photon driven sheet breaking of reduced graphene oxide for amplified light transmission and dust repellent coating, *Applied Materials Today*, 36 (2024) 102012.